Size distribution and energy spectrum in the mixed state induced by Rayleigh-Taylor instability

G. Hazak
Berkeley Research Associates, Inc., Springfield, Virginia 22150, USA
and Physics Department, Nuclear Research Center, Negev, Beer Sheva, Israel

Y. Elbaz
Physics Department, Nuclear Research Center, Negev, Beer Sheva, Israel

J. H. Gardner, A. L. Velikovich, A. J. Schmitt, and S. T. Zalesak
Naval Research Laboratory, Washington, D.C., USA

(Received 19 July 2005; revised manuscript received 13 February 2006; published 26 April 2006)

A study—based on simulations and experiments as well as analytical derivations—of the internal structure of the fragmented ("mixed") state induced by the Rayleigh-Taylor instability at the interface between two fluids is presented. The distribution of sizes and the energy spectrum in the fragmented state are derived from the symmetries exhibited by the data and by dimensional analysis.

DOI: 10.1103/PhysRevE.73.047303 PACS number(s): 47.20.Ky, 47.20.Ma

I. INTRODUCTION

Mixing process induced by hydrodynamic instabilities, such as the Rayleigh-Taylor (RT) instability [1] at the interface between two materials, occurs in a large variety of natural and laboratory systems. Some examples are supernovae, inertial confinement fusion (ICF) pellet implosions, and shock tubes [2].

The RT instability occurs when a light fluid supports a heavier one against gravity, or pushes it with a constant acceleration [1]. Initially, random perturbations at the interface grow exponentially in time. In the nonlinear stage of the instability, round "bubbles" of light fluid enter the heavy fluid and narrow "spikes" of heavy fluid penetrate the lighter one. Later on the "bubbles-spikes" structure breaks down, the interface between the phases becomes distorted [3–9] and the fluid volume becomes very fragmented (for example, see Fig. 1 below). Eventually, a transition to a new state occurs (mixing transition [10]), where molecular mixing becomes the dominant effect. In the present work, we focus on the internal structure of the fluid state before molecular mixing becomes the dominating effect. We shall refer to this late nonlinear stage—just before the mixing transition—as the fragmented state. In some places, we shall use the more familiar term mixing or mixed state. This however should not be confused with the molecular mixing process. For simplicity, we will consider planar geometry and a two-dimensional system with the initial interface perpendicular to the z axis (height). In this geometry, the mixing process proceeds along the z direction, and the system may be assumed to be statistically homogeneous along the y axis. Our analysis relies on the measured phase function [14] $X(y,z,t)$ which is 1 for (y,z) within the heavy fluid and 0 elsewhere. We shall analyze the statistical properties of the system by averaging along the y direction at fixed height z, and denote this process by angular brackets, i.e., $\langle\cdots\rangle \equiv \frac{1}{L}\int_0^L \cdots dy$, where L is the y extension of the system. This analysis applies also to two-dimensional (2D) cuts of a three-dimensional (3D) system, in cases where the averages are invariant to rotation around the z axis, the distribution of sizes drops fast enough as a function of sizes so that aliasing [11] is negligible, and at late stages when inherent 3D effects, such as vortex stretching [15], are not important. The fraction of y axis which is occupied by the heavy fluid, $\alpha(z,t)$, and the autocorrelation of the phase function are obtained by averaging, $\alpha(z,t)=\langle X\rangle$ and $C(\Delta,z,t)\equiv\langle X(y+\frac{\Delta}{2},z,t)X(y-\frac{\Delta}{2},z,t)\rangle$, respectively. Clearly, $\alpha(z,t)=C(0,z,t)$. Experiments [6], dimensional analysis, and direct numerical simulations (DNS) results [3] show that α evolves in a self-similar way, i.e., $\alpha(z,t)=\alpha\left(\frac{z}{\ell(t)}\right)$, where $\ell(t)$ is the z extension of the mixing zone. Dimensional analysis shows that since the system loses the memory of the initial conditions, ℓ must evolve as gt^2 (where g is the gravitational acceleration) multiplied by a dimensionless factor [3]. It is believed that any scalar field will be advected by the velocity field in a way that its concentration power spectrum (e.g., Fourier transform of C with respect to Δ) will have the same functional form as the velocity power spectrum [11,12]. The DNS results for the RT instability show late-time spectra with a non-negligible curvature on log-log scale for which, however, the Kolmogorov power law of $-5/3$ may be a reasonable fit [7,8]. The present work uses the results of DNS and the bilevel images of linear

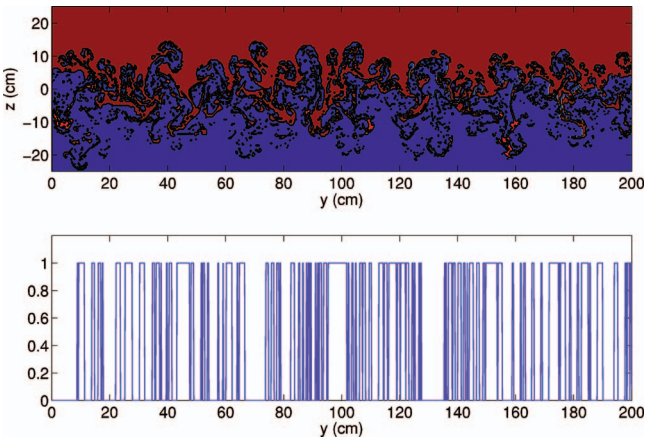

FIG. 1. (Color) Upper frame: The phase function $X(y,z,t=20\ \mathrm{s})$. Lower frame: a cut of Z at $z=0$.

electric motor (LEM) experiments [6]. In our analysis, rather then trying to fit a power law, we looked for symmetries in various moments of the correlation function. The symmetries exhibited by the data allowed us—by an elementary logical process—to find the explicit form of the correlation (and the power spectrum) as a function of size Δ (or wave vector k), height z, and time, t. The energy spectrum is obtained by assuming the same functional dependence on the wave vector. A derivation of a relation between the correlation function (or equivalently, the power spectrum) and the distribution of sizes is presented in Sec. II. Section III contains a description of the three observed symmetries which form the basis for our analysis. Section IV follows with the analysis which leads us to a formula of the correlation function in terms of its lowest moment and additional dimensional considerations which further determine the parameters in the formula and also yield the energy spectrum. A summary and discussion is given in Sec. V.

II. DISTRIBUTION OF SIZES AND CORRELATION FUNCTION

The top frame in Fig. 1 shows the phase function $X(y,z,t)$ at a time during the fragmented stage. The brown area signifies the heavy fluid; and the blue, the light fluid. A cut of the phase function at a specific height z^* is shown in the bottom frame. It is comprised of a sequence of square functions of unit amplitude, of width Δ_m centered at c_m, i.e., $X(y,z,t)=\Sigma_{m=1}^{N_s}\left[\theta\left(y-c_m-\frac{\Delta_m}{2}\right)-\theta\left(y-c_m+\frac{\Delta_m}{2}\right)\right]$, where N_s is the number of segments at z,t and θ is the Heaviside step function [16].

The Fourier transform of X, multiplied by its complex conjugate, immediately yields the exact form of the power spectrum (i.e., Fourier transform of C) in terms of c_m and Δ_m, i.e., $\tilde{X}(z,k,t)\tilde{X}(z,k,t)^*=4\Sigma_{m,m'=1}^{N_s}e^{ik[(c_m-c_{m'})/2]}\frac{1}{k^2}\sin\left[k\left(\frac{\Delta_m}{2}\right)\right]\sin\left[k\left(\frac{\Delta_{m'}}{2}\right)\right]$.

For systems which are statistically homogeneous in the y direction, random phase cancellation kills the $m\neq m'$ terms in the double sum. The inverse Fourier transform of the above relation, for this case, yields

$$f(\Delta,z,t)=\frac{d^2}{d\Delta^2}C(\Delta,z,t)+2\left(\frac{1}{L}\right)N_s(z,t)\delta(\Delta), \tag{1}$$

where $fd\Delta=\int_{\Delta-d\Delta/2}^{\Delta+d\Delta/2}[\Sigma_{m=1}^{N_s}\delta(\Delta'-\Delta_m)]d\Delta'$ is the number of segments (per unit height) of a size in the range $[\Delta-d\Delta/2,\Delta+d\Delta/2]$, at a specific height z and time t. Clearly, for small ensembles and inhomogeneous systems where the random phase cancellation is incomplete, the correlation function carries information about both the size, Δ_m, and the position, c_m, and is not directly related to the distribution of sizes f. This should be taken into account when using correlations measured in experiments or simulations to probe the mixed state. Whenever possible, it is safer to measure the sizes and build the histogram (distribution). In the present work, we will base our analysis on f and then use relation (1) to evaluate the more familiar correlation and power spectrum.

III. OBSERVED SYMMETRIES

The analysis in the present work uses three observations related to symmetries of the distribution function f. The three observations are as follows:

(a) The first observed symmetry involves the well known fact that the integrated volume fraction $\alpha(z,t)$ evolves in a self-similar way, i.e., $\alpha(z,t)=\frac{1}{L}\int_0^\infty f(\Delta,z,t)\Delta d\Delta=\alpha\left(\frac{z}{\ell(t)}\right)$. This was found in many theoretical analyses as well as simulations and experiments (e.g., [3,6]).

Figures 2 and 3 describe the two other symmetries obtained from the phase function extracted from DNS of RT instability in incompressible fluids and from the LEM experiment. The gravitation constant was 1 cm/s^2 in the simulations and 73 times greater than earths gravity in the experiment. The difference in the densities of the light and heavy fluids divided by the sum (i.e., the Atwood number) was 0.5 in the simulations and 0.34 in the experiment.

The observed properties described in Figs. 2 and 3:

(b) Projecting the distribution onto the Δ,t plane by integration dz over the whole mixing region at different times and dividing by its maximum (over all values of Δ) results in a time independent function of Δ, which cannot be represented as a single power of Δ, i.e., $\frac{\int f(\Delta,z,t)dz}{\max_\Delta[\int f(\Delta,z,t)dz]}=a(\Delta)$. This function evaluated at $t=15$, 25, and 31 s in the simulation and the two late frames in the experiments is shown in Fig. 2 The extension of the mixing zone was changed between these times by a factor of ~ 2. Note that DNS and LEM share the same function $a(\Delta)$. This is in spite of the fact that our DNS simulates a 2D system, while the bilevel images of LEM represent 2D cuts of 3D experiments. We have added also a curve of $(\Delta/\Delta_0)^{-1.41}$. Note that this curve is closed to $a(\Delta)$ in the small Δ range over one decade of values of $a(\Delta)$, while the time independence property holds over the whole range [more than two decades of values of $a(\Delta)$].

(c) Define the scales of length $\lambda_n\equiv\frac{\int f\Delta^{n+1/2}d\Delta}{\int f\Delta^{n-1+1/2}d\Delta}$. We have found that, over a relatively large values of z, the various scales are related to each other as

$$\lambda_n=n\lambda_1. \tag{2}$$

This is shown in Fig. 3 for $n=1,2,3$, and 4.

Actually, replacing 1/2 with another number between 0.25 to 0.75 gives a similar result, so in the analysis below we shall use the definition: $\lambda_n\equiv\frac{\int f\Delta^{n+r}d\Delta}{\int f\Delta^{n-1+r}d\Delta}$, and treat r as a parameter which has to be determined by imposing additional physical requirements.

IV. ANALYSIS

The most general form of f, which is consistent with the observed property (a), is

$$f(\Delta,z,t)=\frac{d_0}{d(z,t)^2}q\left(\frac{\Delta}{d(z,t)},\theta\right), \tag{3}$$

where $\theta(z,t)\equiv\frac{z}{\ell(t)}$, d is a function of z and t having a dimension of length, and d_0 is a constant scale length.

Starting with function (3), we have: $\int f(\Delta,z,t)dz=\ell(t)\int\frac{d_0}{d(\theta,t)^2}q\left(\frac{d_0}{d(\theta,t)}\theta\right)d\theta$. Now if d has an explicit depen-

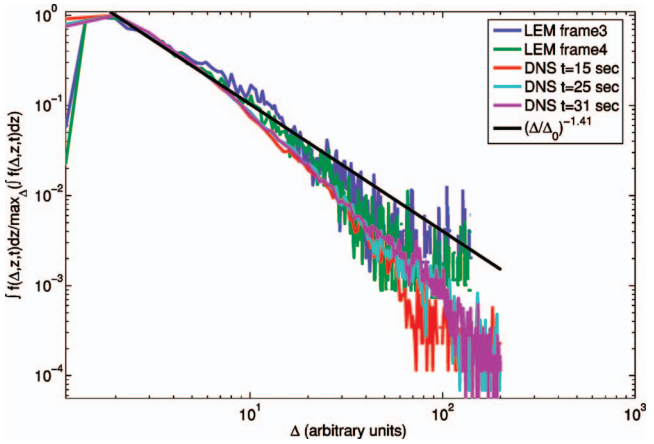

FIG. 2. (Color) Observed symmetry (b); $\frac{\int f(\Delta,z,t)dz}{\max_\Delta(\int f(\Delta,z,t)dz)}$ as function of Δ at $t=15$ s, $t=25$ s, and $t=31$ s, in the DNS, the two later frames in the experiment and a fit for small Δ; $(\Delta/\Delta_0)^{-1.41}$.

dence on t—in addition to the dependence on θ—and the integral above is not a single power of $\frac{\Delta}{d}$, then it will depend on t in a way which cannot be eliminated by dividing by a function of time. So, we conclude that observation (b) implies that the function d must have the form: $d(z,t)=b_0 b(\theta)$, where b_0 is a *time independent* scale of length and b is a dimensionless function. In other words, the most general form of a distribution which is consistent with observations (a) and (b) is

$$f(\Delta,z,t) = R\left(\frac{\Delta}{b_0 b(\theta)},\theta\right). \tag{4}$$

Dividing both sides of relation (2) by λ_1 and using the definition of λ_n it takes the form $\frac{\int_0^\infty(\Delta/\lambda_1)^{n+r}fd(\Delta/\lambda_1)}{\int_0^\infty(\Delta/\lambda_1)^{n-1+r}fd(\Delta/\lambda_1)}=n$, i.e., the ratio of the moments of f with respect to $\xi=\Delta/\lambda_1$ is independent of θ, which is possible only if f may be factored into a function of θ multiplied by a function of ξ. The last conclusion is consistent with the conclusion described in Eq. (4) with $b_0 b=\lambda_1$. Moreover, property (c) may be recognized as the property of the factorial or Gamma function [16], i.e.,

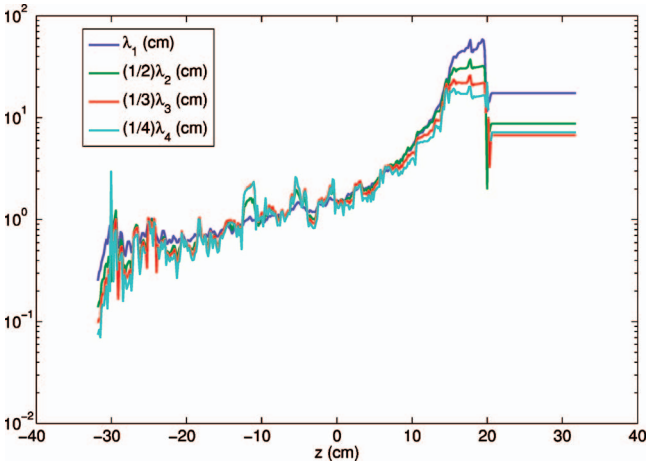

FIG. 3. (Color) $\frac{1}{n}\frac{\int f\Delta^{n+1/2}d\Delta}{\int f\Delta^{n-1+1/2}d\Delta}$ as function of z for $n=1,2,3$, and 4 in the DNS.

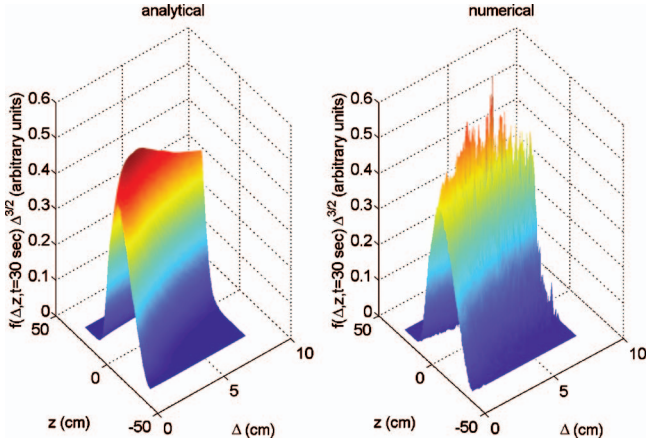

FIG. 4. (Color) Analytical and numerical distribution of sizes at $t=30$ s.

$\frac{\Gamma(n+1)}{\Gamma(n)}=\frac{\int_0^\infty e^{-\xi}\xi^n d\xi}{\int_0^\infty e^{-\xi}\xi^{n-1}d\xi}=\frac{\int_0^\infty \frac{e^{-\xi}}{\xi^r}\xi^{n+r}d\xi}{\int_0^\infty \frac{e^{-\xi}}{\xi^r}\xi^{n-1+r}d\xi}=n$. In other words, we have found a function which obeys the observed property (c), i.e., $f=\phi\frac{e^{-\xi}}{\xi^r}$, where the normalizing prefactor ϕ is a function of θ which is easily found by the requirement that the integrals of f yield α and λ_1.The final result is

$$f = \frac{1}{\Gamma(2-r)}\frac{L}{\lambda_1^2}\alpha\frac{e^{-\xi}}{\xi^r}. \tag{5}$$

Figure 4 demonstrates the capacity of Eq. (5) which was obtained by a deductive process from properties (a)–(c) to return the numerical data. This is done by comparing the analytical form of the distribution, assuming $r=1/2$ (left frame in Fig. 4 which was plotted by using the value of λ_1 from the simulation) with the distribution obtained directly from the simulation (right frame in Fig. 4).

The physical meaning of the scale λ_1 may be explained as follows: The moments of the distribution are; $(\bar{\Delta}^p)\equiv\frac{\int_0^\infty f\Delta^p d\Delta}{\int_0^\infty f d\Delta}=\frac{\Gamma(p+r)}{\Gamma(r)}(\lambda_1)^p$. In particular for $p=1$, we have $\bar{\Delta}=r\lambda_1$. Since the derivative of $X(y,z,t)$ represents a delta function at interface [13,14], integration along a line will

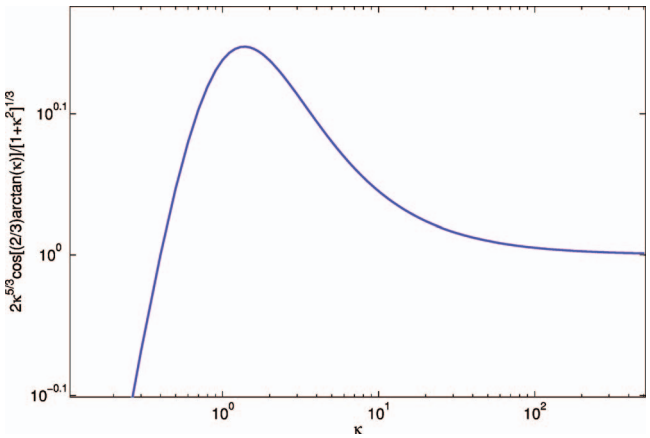

FIG. 5. (Color) The ratio between the spectrum and the Kolmogorov law for the κ behavior in the inertial range.

count the number of times that the line crosses the interface, i.e., the number of segments may be written as $\frac{1}{L}N_s = \frac{1}{2}\left\langle \left| \frac{\partial X(y,z,t)}{\partial y} \right| \right\rangle$ and λ_1 may be written as $\lambda_1 = 2r\frac{\langle X \rangle}{\langle |\partial X/\partial y| \rangle}$. In regions where the small scales dominate, most of the gradients in the velocity come from the sharp transition at the interface, so, for every component of the velocity, one may approximate $\vec{\nabla}(Xu) \sim u\vec{\nabla}X$ and $\lambda_1 \sim 2r\frac{\langle uX \rangle}{\langle |\partial(uX)/\partial y| \rangle}$, which may be recognized as the definition of the Taylor microscale [15]. We did not yet identify the time independent scale of length which enters in the scale λ_1 [b_0 in Eq. (4)]. This may be obtained from dimensional considerations, since the only time independent factors in the problem are the viscosity ν and gravity constant g, from which the only time independent combination with a dimension of length is: $b_0 = \left(\frac{\nu^2}{g}\right)^{1/3}$.

The density power spectrum (i.e., the cosine Fourier transform of $\frac{C(\Delta,z,t)-C(0,z,t)}{C(0,z,t)}$) is readily found by using relations (1) and (5):

$$S(k,z,t) = \lambda_1^2 N_s \sqrt{\frac{2}{\pi}} \Gamma(1-r) \frac{\cos[(1-r)\arctan(\kappa)]}{\kappa^2[1+\kappa^2]^{(1-r)/2}}, \quad (6)$$

where $\kappa \equiv k\lambda_1$. For 3D experiments with isotropy in the x,y plane, considering a ring of κ values $2\pi\kappa d\kappa$, we have to multiply this result by $2\pi\kappa$. For $\kappa < 1$ the spectrum behaves as κ^{-1}, for $\kappa > 1$ it drops as $\kappa^{-(2-r)}$.

Assume that the energy spectrum has the same dependence on κ as the power spectrum of the phase function [12,8], i.e., $E(k,z,t) = E_0 \frac{\cos[(1-r)\arctan(\kappa)]}{\kappa^2[1+\kappa^2]^{(1-r)/2}}$, where E_0 has the dimension of [velocity]^2[length]. For $\kappa \ll 1$ the energy spectrum will behave as $\frac{E_0}{kb_0b(\theta)}$, and for $\kappa \gg 1$ as $\frac{E_0}{[kb_0b(\theta)]^{2-r}}$. The energy budget in the RT system is governed by the dissipation rate ε which depends on z and t, the viscosity ν, and the gravity constant g. We assume a simple monomial for E_0; $E_0 = \beta\nu^{r_1}g^{r_2}\varepsilon^{r_3}$, where β is a dimensionless constant. The requirement that this form will result in the right dimension, together with the requirement, that the spectrum at $\kappa \gg 1$ will be independent of both the viscosity and the gravity will yield four algebraic equations for r, r_1, r_2, and r_3. The solution yields $r = 1/3$, and

$$E(k,z,t) = \beta\varepsilon^{2/3}\left(\frac{\nu^2}{g}\right)^{5/9} \frac{\cos\left[\frac{2}{3}\arctan(\kappa)\right]}{\kappa[1+\kappa^2]^{1/3}}. \quad (7)$$

At large κ, this spectrum drops as $\kappa^{-5/3}$. The deviation at intermediate values of κ from the Kolmogorov $\kappa^{-5/3}$ law for the energy spectrum at the inertial range in homogeneous turbulence is shown in Fig. 5, where the ratio $2\kappa^{5/3}\frac{\cos[(2/3)\arctan(\kappa)]}{\kappa[1+\kappa^2]^{1/3}}$ is plotted. As mentioned above, the spectrum in a 2D system would differ by a factor $2\pi\kappa$.

V. SUMMARY AND DISCUSSION

The main results of the present work are in relation (1) between the correlation and distribution of sizes, the explicit form of distribution of sizes (5), the density power spectrum (6), and the energy spectrum (7). These functions are written in terms of the average size $\lambda_1 = 2\bar{\Delta} \equiv 2\frac{\int_0^\infty f\Delta d\Delta}{\int_0^\infty f d\Delta} = 2\frac{\alpha}{N_s}$ (at heights at which the small scales dominate λ_1 coincides with the Taylor microscale). It was also found that this scale behaves in a self-similar way; $\lambda_1 = b_0 b(\theta)$. Further dimensional considerations show that the scale of length is $b_0 \sim \left(\frac{\nu^2}{g}\right)^{1/3}$ (which is the wavelength of the fastest growing mode [17,18]). The physical origin of the found symmetries, (a) and (b), may be traced to the memory loss of the initial conditions, i.e., in the absence of a characteristic scale of length of the order of the size of the mixing zone, the system will evolve in a self-similar way. All profiles (α, d, etc.) will depend on z,t only through the combination $\theta \equiv \frac{z}{\ell(t)}$ [3,15,11]. Form (4) is the only form of the distribution of sizes which yields such profiles. We could not find a simple physical explanation for observation (c). The fact that it uniquely determines the distribution of sizes as a Gamma distribution, $\frac{e^{-\xi}}{\xi^r}$ [16] [see Eq. (5)] may indicate that it is related to the tendency of the system to maximize entropy. This topic is beyond the scope of the present work. Further studies are also needed in order to asses the generality of the results beyond the RT mixing problem. This may be achieved by using our method to extract the distribution from symmetries in a large variety of experiments and DNS of turbulent mixing layers (e.g., jet and wake flows [15]).

ACKNOWLEDGMENT

The authors thank Guy Dimonte for supplying the data from the LEM experiments and for helpful discussions.

[1] G. I. Taylor, Proc. R. Soc. London, Ser. A **201**, 192 (1950).
[2] Y. Zhou *et al.*, Phys. Plasmas **10**, 1883 (2003).
[3] D. L. Youngs, Physica D **12**, 32 (1984).
[4] D. L. Youngs, Physica D **37**, 270 (1989).
[5] D. L. Youngs, Laser Part. Beams **12**, 725 (1994).
[6] M. B. Schneider *et al.*, Phys. Rev. Lett. **80**, 3507 (1998).
[7] G. Dimonte *et al.*, Phys. Fluids **16**, 1668 (2004).
[8] S. B. Dalziel *et al.*, J. Fluid Mech. **399**, 1 (1999).
[9] M. Chertkov, Phys. Rev. Lett. **91**, 115001 (2003).
[10] P. Dimotakis, J. Fluid Mech. **409**, 69 (2000).
[11] H. Tennekes and J. L. Lumley, *A First Course in Turbulence* (MIT Press, Cambridge, MA, 1972).
[12] S. Corrsin, J. Appl. Phys. **22**, 469 (1949).
[13] K. R. Sreenivasan, Annu. Rev. Fluid Mech. **23**, 539 (1991).
[14] D. A. Drew, Annu. Rev. Fluid Mech. **15**, 261 (1983).
[15] P. A. Davidson, *Turbulence* (Oxford University Press, Oxford, UK, 2004).
[16] G. Arfken, *Mathematical Methods for Physicists* (Academic, New York, 1985).
[17] Ya. B. Zeldovich and Yu. P. Raizer, *Physics of Shock Waves and High-Temperature Hydrodynamic Phenomena* (Dover, New York, 2002).
[18] S. Chandrasekhar, *Hydrodynamic and Hydrodynamic Stability* (Dover, New York, 1981).